Electronic Supplementary Material (ESI) for Materials Advances.

SUPPLEMENTARY INFORMATION

Innovative Strategies for Nitrogen-Incorporated Silicon oxycarbide-Based Preceramic Polymers Synthesis

B. Pérez-Román[1*], A. Merchán del Real[2], J. Rubio[1], M. A. Mazo [1], F. Rubio-Marcos[1]

[1] *Ceramic and Glass Institute (ICV-CSIC), Kelsen St. 5, 28049, Madrid, Spain*
[2] *Organic Chemistry Department, Faculty of Science, Autonomous University of Madrid, Francisco Tomás y Valiente 7, 28049, Madrid, Spain*

*__Authors to whom correspondence should be addressed__. B. P-R: Phone: +34 91 735 58 40 Fax: +34 91 735 58 43. Email: berta.perez@icv.csic.es

Keywords: Synthesis, Nitrogen, Dendron, Doping, silicon oxycarbide

S1 Characterization of the synthesized TRIAZ-3 structure: N^2, N^4, N^6-tris (4-vinyl phenyl)-1,3,5-triazine-2,4,6-triamine.

The commencement of our investigation is marked by the precise synthesis of TRIAZ-3, followed by an exhaustive exploration of its properties through a judicious combination of advanced analytical techniques. Employing a methodical approach, we harnessed the power of one-dimensional NMR (^{1}H and ^{13}C) **–Figure S1 and S2-** and DEPT-135 **-Figure S3-** to dissect the molecular intricacies of TRIAZ-3.

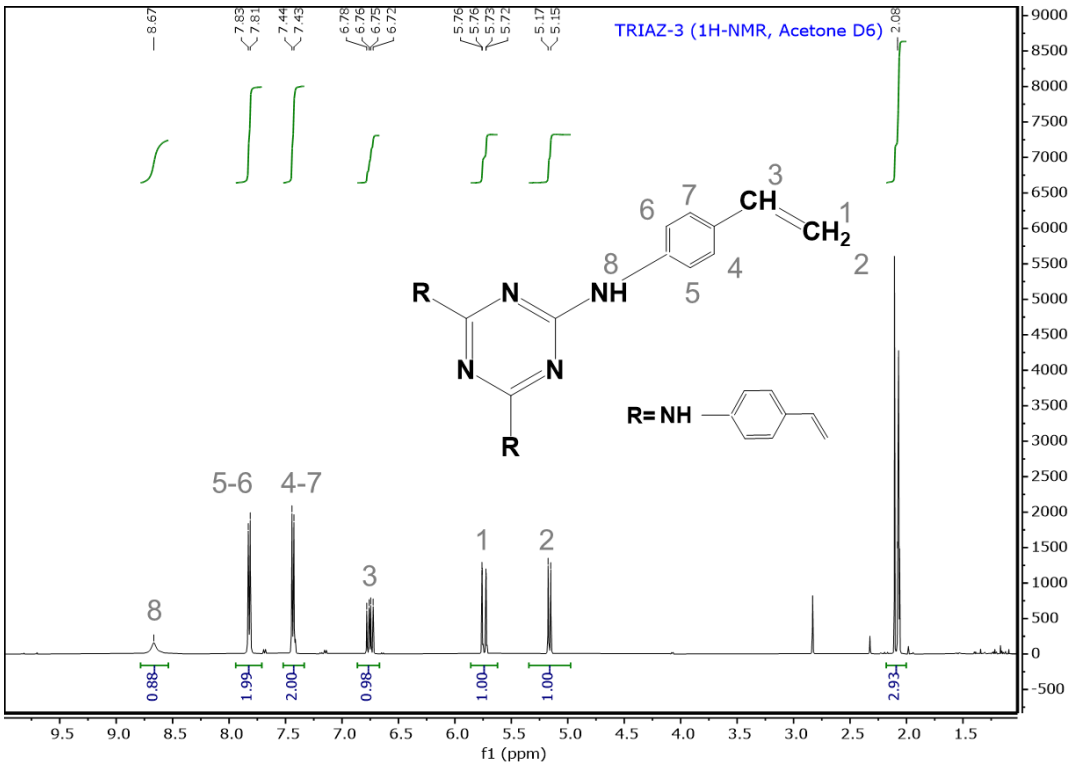

Figure S1 | ^{1}H-NMR Spectra of TRIAZ-3 Structure. This spectrum reveals the distinctive signals corresponding to the various protons within the TRIAZ-3 molecule, providing a comprehensive illustration of the synthesized dendron's structural characteristics. Notice that signal presented in 2.93 ppm is related with the Acetone-D6 employed for the NMR measurements.

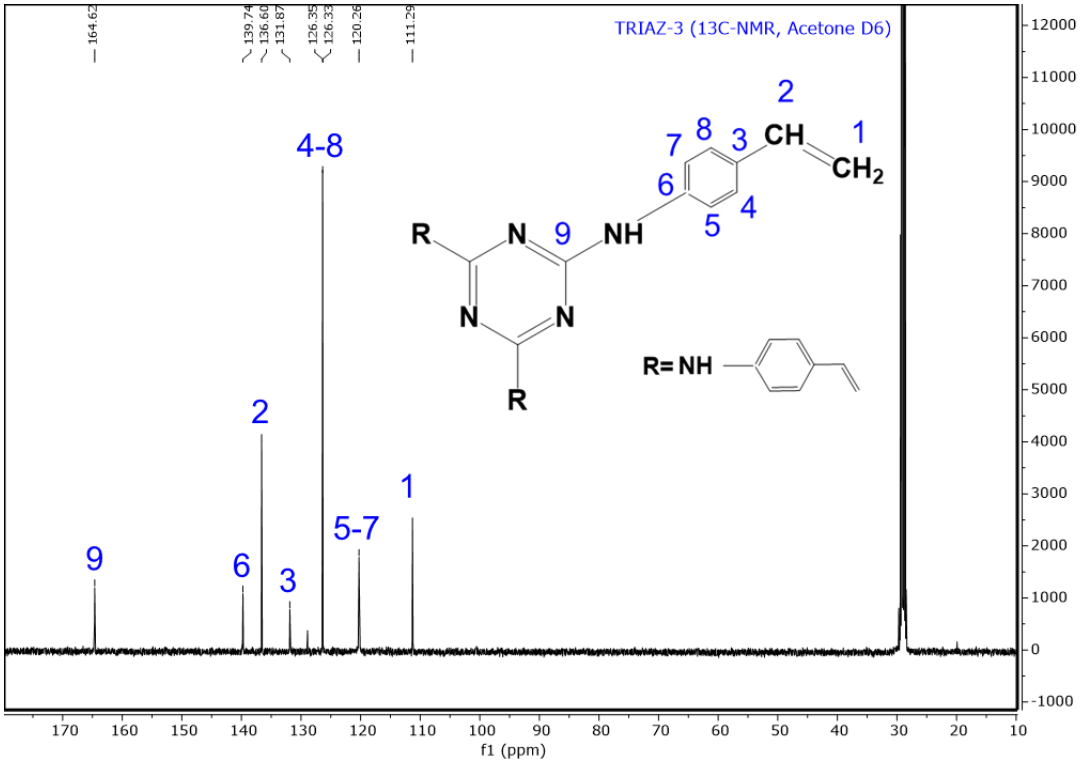

Figure S2 | ^{13}C-NMR Spectra of TRIAZ-3 Structure. The spectrum presents a detailed mapping of carbon resonances within the TRIAZ-3 dendron, with individual carbon elements labeled numerically from 1 to 9. This numbering facilitates the association of each signal with its respective carbon site, elucidating the intricate structural configuration of the synthesized dendron.

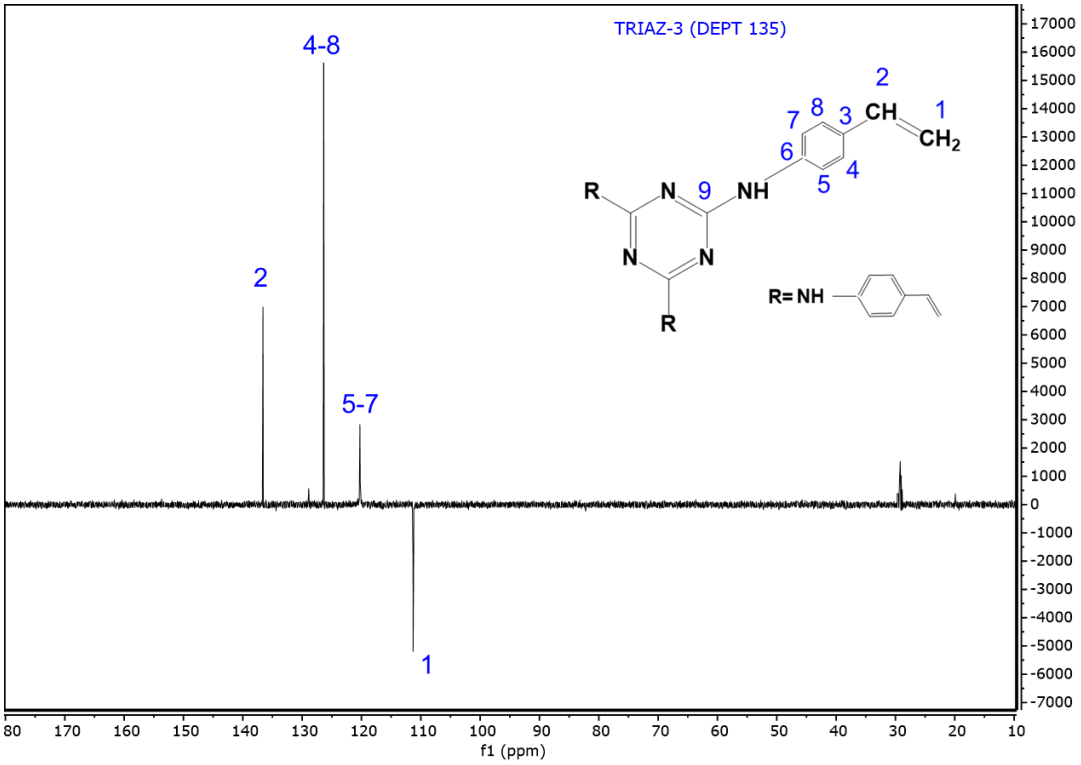

Figure S3 | DEPT-135 ^{13}C NMR Spectra of TRIAZ-3 Structure. This spectrum plays a crucial role in identifying and characterizing the resonance signals showcased in **Supplementary Figure S2.** It provides a clear distinction between primary, secondary, and tertiary carbons within the TRIAZ-3 dendron. Notably, CH_3 and CH-related resonances are presented in an upright orientation, while CH_2 resonances appear inverted. This comprehensive analysis aids in unraveling the intricate carbon framework and connectivity of the synthesized dendron, further enhancing our understanding of its structural intricacies.

S2 Structural characterization of pyrolyzed polymeric precursor (AHPCS) by means of FTIR

The spectral analysis of pyrolyzed AHPCS across different temperature ranges involved an initial deconvolution process, where Gaussian bands were extracted. These bands served as a preliminary approximation for characterizing the TZPC20 and TZPC48 samples. An illustrative demonstration of this meticulous process is thoughtfully presented in **Figure S4**, offering valuable insights into the intricacies of spectral analysis.

For a comprehensive understanding of the spectral data, detailed information regarding the positions, Full Width at Half Maximum (FWHM), and areas of the distinct bands is meticulously documented in **Table S1.**

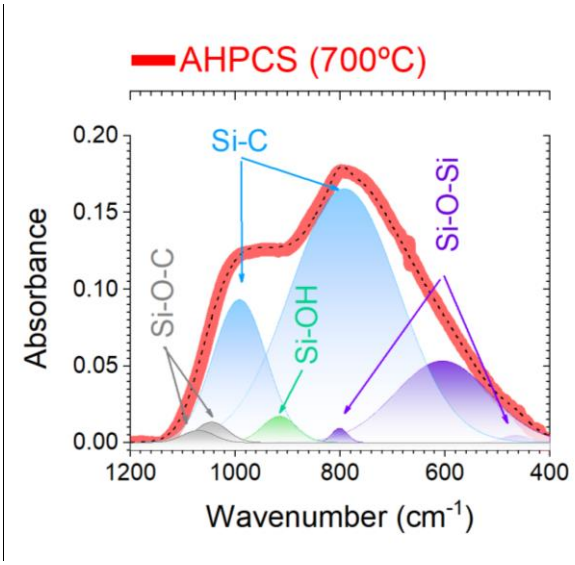

Figure S1 | FTIR spectra and its corresponding deconvolution of the AHPCS pyrolyzed at 700 °C. This figure offers a detailed view of the spectral range spanning from 1200 to 400 cm^{-1} and the precise deconvolution process that follows. Within this deconvolution, distinct Gaussian curves are thoughtfully distinguished, each representing specific bands associated with Si-O, Si-C, and Si-OH bonds—integral components of the ceramic structure.

Data obtained from the deconvolution of FTIR spectra										
Samples		**δ (O-Si-O)**		**υ(Si-C-Si)**	**υ(Si-O-Si)**	**(Si-C-Si)**	**υ(Si-N)**	**Si-OH**	**Si-O-C/Si-O-N**	
AHPCS-700	Position	465	605	792	801	992		**916**	1045	1070
	Intensity	0.003	0.120	0.425	0.004	0.119		0.014	0.010	0.006
	Width	50	180	205	30	102		66	60	60
	Area	0.16	23.04	92.94	0.11	12.95		1.00	0.64	0.38
AHPCS-900	Position	470	606	793	801	980		**905**		
	Intensity	0.006	0.165	0.555	0.004	0.058		0.025		
	Width	50	177	200	30	85		70		
	Area	0.32	31.15	118.41	0.11	5.26		1.87		
TZPC20-700	Position	463	598	787	801	1016	938		1040	1095
	Intensity	0.004	0.048	0.350	0.003	0.135	0.023		0.002	0.011
	Width	52	150	215	29	113.5	78		60	71
	Area	0.19	7.68	80.27	0.08	16.35	1.87		0.13	0.83
TZPC48-900	Position	472	608	792	801	1014	942			1080
	Intensity	0.004	0.058	0.343	0.006	0.031	0.036			0.002
	Width	60	172	223	40	80	102			50
	Area	0.24	10.64	81.60	0.26	2.65	3.92			0.09

Table S1 | Data extracted from the deconvolution of the FTIR spectra of the AHPCS pyrolyzed at 700 and 900 °C, and the samples TZPC20-700 and TZPC48-900. This comparative analysis encompasses the two extremes of the synthesis conditions, aiming to elucidate the microstructural transformations within the ceramic materials during their formation. The data presented in this table serves as a valuable resource for comprehending the evolving structure of the ceramic materials throughout the synthesis process. Notably, it highlights the formation of new Si-N bonds, a consequence of the incorporation of the TRIAZ-3 dendron into the ceramic framework. Moreover, this data sheds light on the progressive development of Si-N bonds with increasing treatment temperatures, underscoring the significance of temperature control in tailoring the material's structural attributes.

S3 Structural characterization by means of XPS of the prepared SiOCN ceramic material, TRIAZ-3 and pyrolyzed AHPCS

In this dedicated section, we embark on a comprehensive investigation of the surface properties exhibited by the pyrolyzed materials, employing the powerful analytical tool of XPS. This sophisticated technique proves instrumental in providing profound insights into the electronic core levels, including C1s, O1s, N1s, Si2s, and Si2p. Moreover, it encompasses the evaluation of Auger bands, offering a holistic perspective on the elemental composition and electronic states present within the pyrolyzed materials. The discerning utilization of XPS, enabling a deeper understanding of the intricate surface chemistry and electronic interactions within these innovative materials. For a comprehensive visual representation of our findings, readers are directed to **Figure S5**, where the obtained XPS spectra are thoughtfully presented, further enriching our exploration of these intriguing materials.

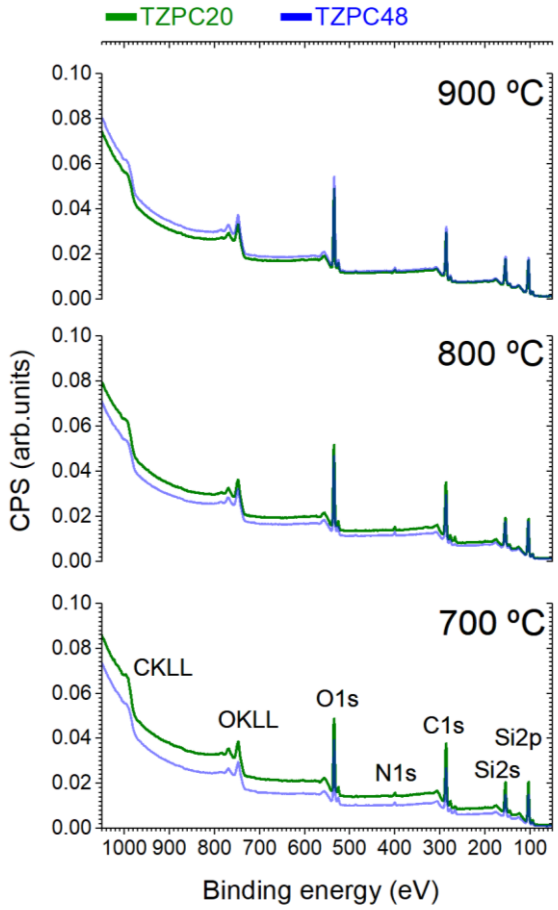

Figure S5 | A comprehensive view of the survey spectra for our pyrolyzed materials. In this figure, the green line represents TZPC20, while TZPC48 is depicted as a series of blue lines. These survey spectra offer a valuable insight into the electronic configurations of the diverse chemical elements that constitute the intricate structures of our ceramic materials. The elemental compositions, which were meticulously calculated and presented in **Table 3** within the main manuscript, find their origins in the spectral data showcased in this figure.

Based on the comprehensive dataset acquired from our XPS analyses, a noteworthy observation emerges. It is reasonable to postulate that the composition of our material exhibits a remarkable degree of homogeneity, extending from the bulk to the surface. This remarkable uniformity in composition leads us to infer that the

bonding types and electronic states identified through our rigorous analyses are faithfully representative of the material's entirety. For a more detailed visualization of our finding, the **Figure S6** and **Figure S7** meticulously showcase the deconvoluted Gaussian bands corresponding to the XPS spectra of two critical components: the as-synthesized dendron TRIAZ-3 and the AHPCS material subjected to a treatment at 900 °C.

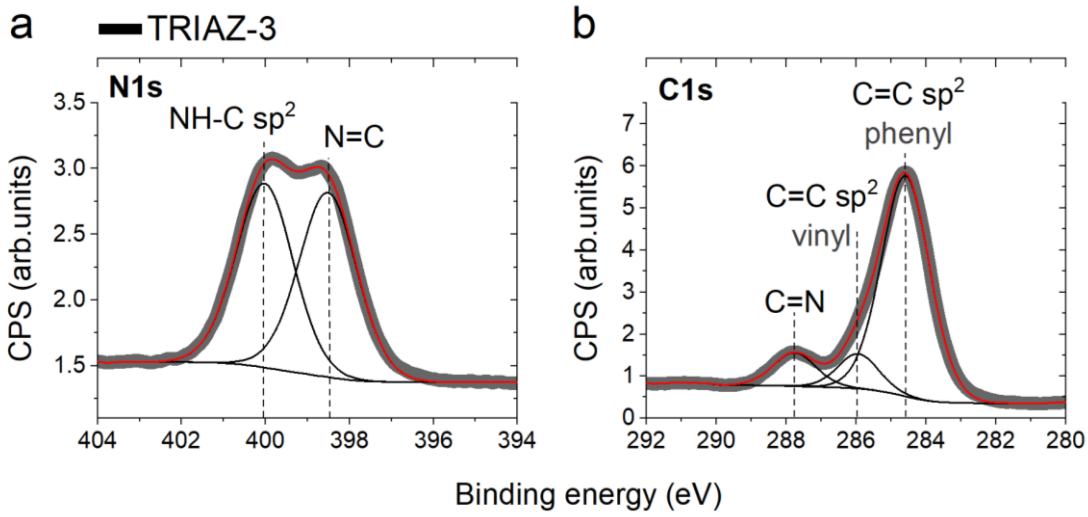

Figure S6 | a. N1s and **b.** C1s XPS spectra of the TRIAZ-3 molecule are presented in this figure**.** The panel **a.** illustrates the distinct features of the N-containing dendron structure. It enables the detection of essential components within the molecule, such as the presence of triazine aromatic rings (N=C)) and the characteristic –NH- bonds that constitute the synthesized dendron (NH-C sp^2). On the other hand, the panel **b.** offers a detailed perspective on the carbon content of the dendron. It is evident from this spectrum that the carbon composition primarily comprises aromatic rings (C=C sp^2 phenyl), followed by the vinyl functional groups (C=C sp^2 vinyl) and the prominent triazine ring (C=N). It is noteworthy that the XPS data corroborate the structural information previously elucidated, as demonstrated by the NMR results showcased in **Supplementary Section 1, Figure S1-3.**

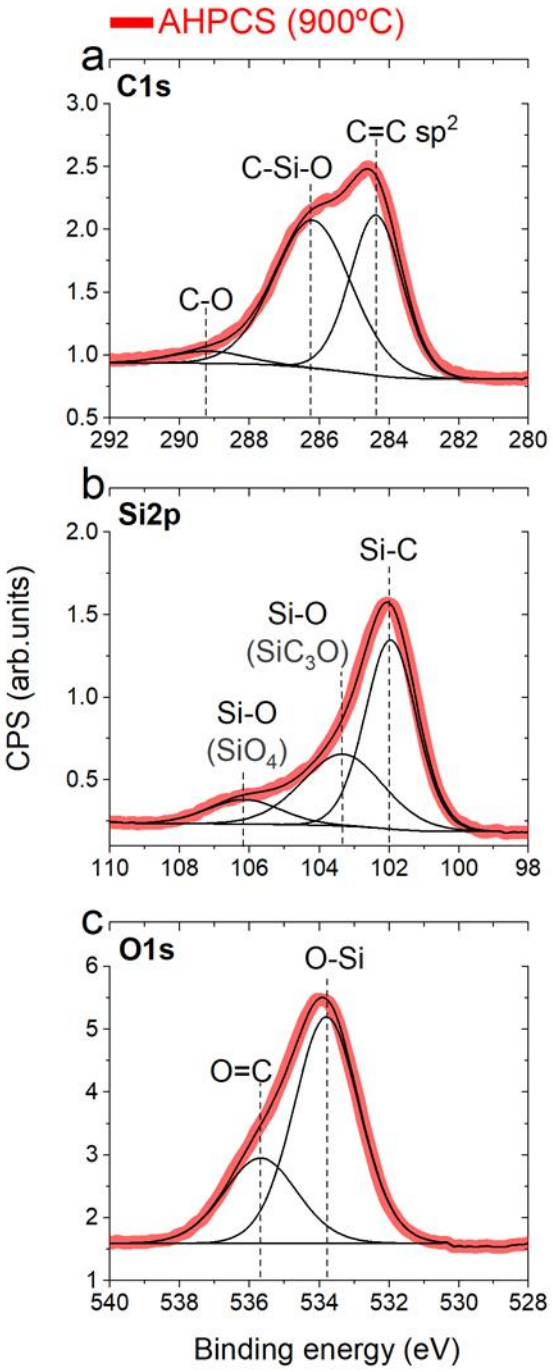

Figure S7 | A set of XPS spectra, including **a.** C1s, **b.** Si2p, and **c.** O1s, obtained from the commercially acquired AHPCS treated at 900 °C under inert atmospheric conditions. These spectra serve as a fundamental reference for understanding the initial structure of the ceramic material derived from the commercial AHPCS. They also represent the starting point for the subsequent deconvolution analysis conducted on the TZPC20 and TZPC48 materials, as depicted in **Figure 5** of the main manuscript.

S4 Analysis of the crystalline phases by XRD of TZPC materials and AHPCS pyrolyzed at different temperatures

To investigate the microstructural characteristics of the prepared SiOCN materials, XRD analyses were conducted on the samples to elucidate the crystalline phases present after the pyrolysis process. AHPCS was initially pyrolyzed in its as-received state, to examine the formation of SiC, which manifested in an amorphous state. AHPCS was pyrolyzed under an argon atmosphere, and pyrolysis temperatures correspond to those used for SiOCN preparation, with an additional spectrum at 1100 ºC, to explore the evolution of the preceramic precursor's microstructure as function of temperature. Furthermore, Figure S8 includes TZPC20-700 and TZPC48-900, showcasing the extremes in reaction time synthesis and pyrolysis temperature.

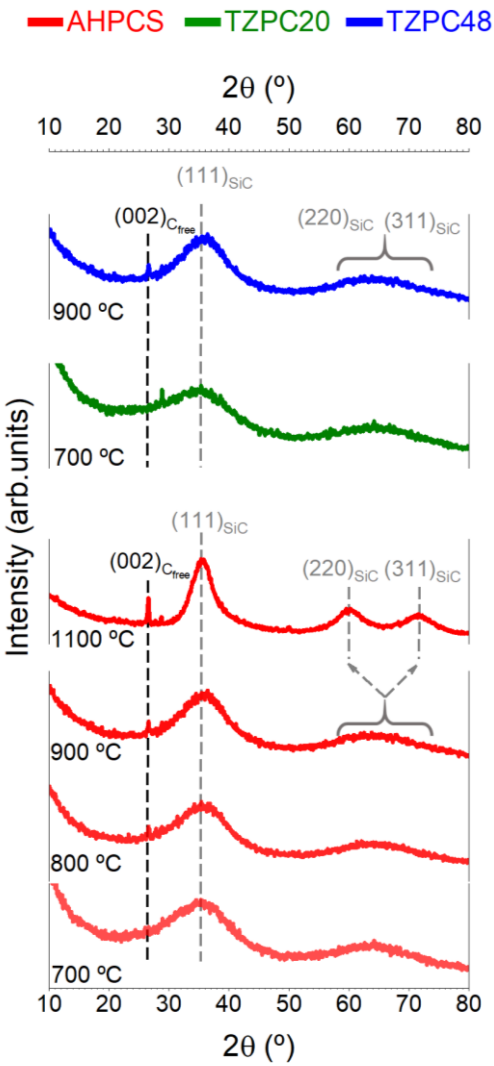

Figure S8 | XRD spectra of the AHPCS preceramic precursor treated at 700, 800, 900 and 1100 ºC under inert atmosphere and TZPC20-700 and TZPC48-900 prepared materials. The displayed curves illustrate the microstructure of the prepared materials, which are fundamentally formed by amorphous SiC, discerning the characteristic lattice planes of SiC at 2θ ≈ 35, 60 and 75º associated to (111), (220) and (311) respectively. At the pyrolysis temperatures employed for the obtention of the TZPC materials, the lattice planes corresponding to (220) and (311) are not still distinguished, observing a broad band at 2θ ≈ 65º representing both contributions. The inherent C_{free} phase of the SiOCN which was previously studied in the manuscript by Raman spectroscopy, is also observed as a

sharp peak located at $2\theta \approx 26^{o}$, representing the ordered graphite phase. The intensity of the C_{free} phase increases with temperature pyrolysis in both in the treated AHPCS and TZPC materials, suggesting higher crystallinity with an elevated temperature treatment.

Structural Analysis: X-ray Diffraction (XRD) analysis utilized the Bruker D8 Discover Theta/2theta instrument with Cu K_{α} radiation (λ = 0.154056 nm) on AHPCS and SiOCN materials. Measurements spanned 5–80° (2θ) at 0.02° intervals for 1 second per step. Employing the Detector 1-D LYNXEYE XE-T ensured high-resolution data, eliminating K_{β} radiation and fluorescence interference.

S5 Microstructural characterization by means of FE-SEM of the newly TRIAZ-3 and prepared SiOCN materials

In this additionally section, the FE-SEM was employed to investigate the microstructure of the recently synthesized TRIAZ-3 and TZPC materials under various synthesis parameters. The micrographs showed in **Figure S9** depict the initial TRIAZ-3 material, along with the TZPC20-700 and TZPC48-900 samples, showcasing the extremes of the synthesis parameters.

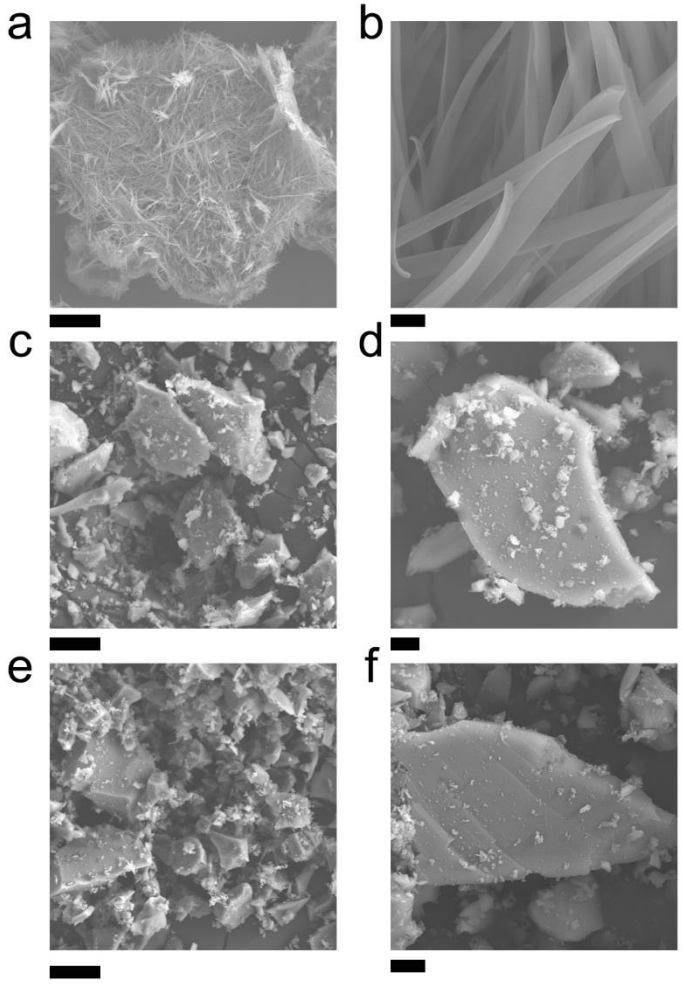

Figure S9 | A group of FE-SEM images corresponding to **a. b.** TRIAZ-3, **c. d.** TZPC20-700 and **e. f.** TZPC48-900. Scale bar for **a. c.** is 50 μm, **d.** is 1 μm and **b. f.** is 5 μm. The dendritic microstructure of TRIAZ-3 presents a ribbon-like structure of different sizes, observing varied widths and thicknesses below 1 μm. In contrast, the prepared TZPC materials showcase polygonal molecules with irregular shapes and smaller aggregates. The ribbon structure of TRIAZ-3 is indiscernible in the TZPC materials, attributed to the low concentration of dendron in the ceramized materials.

Microstructural Analysis: The microstructural analysis of TRIAZ-3 and SiOCN did not involve sample preparation for examining the samples, with the exception of gold sputtering for the non-conductive TRIAZ-3 and SiOCN powders. Samples were examined by using a Hitachi S-4700 Field Emission Scanning Electron Microscopy (FE-SEM) with the aim to study the microstructural features of each material.